Chapter 2

Slab Stress and Strain Rate as Constraints on Global Mantle Flow

Originally published in:

Alisic, L., Gurnis, M., Stadler, G., Burstedde, C., Wilcox, L. C., & Ghattas, O. (2010). Slab stress and strain rate as constraints on global mantle flow. *Geophysical Research Letters*, 37, L22308.

2.1 Abstract

Dynamically consistent global models of mantle convection with plates are developed that are consistent with detailed constraints on the state of stress and strain rate from deep focus earthquakes. Models that best fit plateness criteria and plate motion data have strong slabs that have high stresses. The regions containing the M_W 8.3 Bolivia and M_W 7.6 Tonga 1994 events are considered in detail. Modeled stress orientations match stress patterns from earthquake focal mechanisms. A yield stress of at least 100 MPa is required to fit plate motions and matches the minimum stress requirement obtained from the stress drop for the Bolivia 1994 deep focus event. The minimum strain rate determined from seismic moment release in the Tonga slab provides an upper limit of $\sim$ 200 MPa on the strength in the slab.

2.2 Introduction

An essential component of mantle convection models with plates is the strength of the subducting slabs and their influence on the dynamics of the convective system. The stronger slabs are, the more they could exert an important force on plate motions, acting as stress guides. Regional studies using the geoid concluded that the viscosity in the slabs is 100 to 1000 times higher than in the surrounding mantle (*Moresi and Gurnis*, 1996), and could not exceed 10^{23} Pa s in order to fit geoid highs over subducted slabs (*Billen et al.*, 2003). Also, studies of plate bending indicate that the plate viscosity must be between 50 and 200 times the mantle viscosity in order to fit dissipation constraints (*Conrad and Hager*, 1999a). Torque balance models of the Pacific and Australian plate suggested that the best fit to observed rotation poles was obtained with an effective lithosphere viscosity of 6×10^{22} Pa s (*Buffett and Rowley*, 2006). In contrast, with time-dependent generic models of slab dynamics, strong slabs are inferred (*Billen and Hirth*, 2007), in concordance with experimentally found temperature dependence of the effective viscosity of olivine (*Hirth and Kohlstedt*, 2003). Using a composite rheology with a nonlinear component (*Billen and Hirth*, 2007) allows for localization of strain, and hence localized strain weakening in the hinge of a subducting slab. In this way, slabs can be strong and still subduct with relative ease. Global models addressing slab pull show that strong slabs provide the best fit to observed plate motions, exerting slab pull forces that account for approximately half of the total driving forces on plates (*Conrad and Lithgow-Bertelloni*, 2002).

The state of stress indicated by earthquake focal mechanisms and their stress drop, in selected cases, provide additional constraints on the strength of slabs. The stress drop estimates for large moment magnitude deep earthquakes form a lower limit of the stress that the slab must sustain. Here the state of stress of slabs is studied in globally consistent dynamic models

of mantle convection with plates, while incorporating a composite rheology. We address two study areas, covering the locations of the Bolivia, M_W 8.3, 1994 and the Tonga, M_W 7.6, 1994 earthquakes. These earthquakes were chosen because they putatively represent end member types of deep earthquakes. The Bolivia earthquake experienced a large stress drop of 114 MPa, a rupture propagation of only 1 km/s, few aftershocks, and was located in a region with scarce seismicity (*Kanamori et al.*, 1998). In contrast, the Tonga earthquake had a low stress drop ($\sim$ 1.6 MPa), fast rupture propagation of 3–4 km/s, and many aftershocks in a region with abundant seismicity (*Wiens and McGuire*, 1995).

2.3 Model Setup and Solution

The dynamics of instantaneous mantle convection are governed by the equations of conservation of mass and momentum. Under the Boussinesq approximation for a mantle with uniform composition and the assumption that the mantle deforms viscously, the nondimensionalized form of these equations is (e.g., *Schubert et al.* (2001)):

$$\nabla \cdot \mathbf{u} = \mathbf{0}, \tag{2.1}$$

$$\nabla \mathbf{p} - \nabla \cdot \left[\eta(T, \mathbf{u}) \left(\nabla \mathbf{u} + \nabla \mathbf{u}^{\top} \right) \right] = \mathrm{Ra}\, T\, \mathbf{e}_r, \tag{2.2}$$

where $\mathbf{u}$, $\mathbf{p}$, η, and T are the velocity, pressure, viscosity, and temperature, respectively; $\mathbf{e}_r$ is the unit vector in the radial direction. Ra is the Rayleigh number, $\mathrm{Ra} = \alpha \rho_0 g \Delta T D^3 / (\kappa \eta_0)$, where α, ρ_0, η_0, and κ are the reference coefficients of thermal expansion, density, viscosity, and thermal diffusivity (see Table 3.1). ΔT is the temperature difference across a mantle with thickness D, and g is the gravitational acceleration.

We solve these equations with finite elements using a code (`Rhea`) that exploits Adaptive Mesh Refinement (AMR) (*Burstedde et al.*, 2008a). Rhea is a new generation mantle convection code, using forest-of-octree-based adaptive meshes. With `Rhea`'s adaptive capabilities we create local resolution down to $\sim$ 1 km around plate boundaries, while keeping the mesh at a much coarser resolution away from small features. The global models in this study have approximately 200 million elements, a reduction of a factor $\sim$ 5000 compared to a uniform mesh of the same high resolution (*Stadler et al.*, 2010).

A composite formulation of Newtonian (diffusion creep) and non-Newtonian (dislocation creep) rheology is implemented along with yielding. Plate boundaries are modeled as narrow weak zones with a defined viscosity reduction of several orders of magnitude. A generalized viscosity law for the Earth's mantle is used:

$$\eta = \Gamma(\mathbf{x}) \left(\frac{d^p}{A\, {C_{OH}}^r} \right)^{\frac{1}{n}} \dot{\varepsilon}_{\mathrm{II}}^{\frac{1-n}{n}} \exp\left(\frac{E_a + PV_a}{nRT} \right), \tag{2.3}$$

where η is viscosity in Pa s, d grain size in μm, C_{OH} water content in parts per million of silicon, n the stress exponent, and $\dot{\varepsilon}_{\mathrm{II}}$ the second invariant of the strain rate tensor in s^{-1}. E_a is the activation energy in J/mol, P lithostatic pressure in Pa, V_a activation volume in m^3/mol, R the gas constant, and T the temperature in K. $\Gamma(\mathbf{x})$ is a reduction factor used to define weak zones, and is set to between 10^{-5} and 5×10^{-3} in plate boundaries and to 1 elsewhere. The parameters A, n, r, and p are determined experimentally (*Hirth and Kohlstedt*, 2003). The composite viscosity (*Billen and Hirth*, 2007) is obtained by combining diffusion creep (η_{df}) and dislocation creep (η_{ds}) using a harmonic mean. Then, a yield criterion with yield strength

σ_y is imposed to obtain an effective viscosity:

$$\eta_{\text{comp}} = \frac{\eta_{df}\eta_{ds}}{\eta_{df} + \eta_{ds}}, \tag{2.4}$$

$$\eta_{\text{eff}} = \min\left(\frac{\sigma_y}{\dot{\varepsilon}_{\text{II}}}\ ,\ \eta_{\text{comp}}\right). \tag{2.5}$$

The yielding law is only applied if the local temperature is lower than the yield temperature T_y. See Table 3.2 for a summary of the parameter values used in the presented models.

Since plate velocities and "plateness" are outcomes, both the full buoyancy field and plate boundary details at a fine scale must be incorporated. The global models are constructed with oceanic plate ages (*Müller et al.*, 2008), a thermal model containing slabs in the upper mantle, and tomography in the lower mantle (*Ritsema et al.*, 2004). Current tomography resolves slabs in the upper mantle poorly, as mantle wedges and slabs typically blur together. However, resolving the slabs as high-viscosity stress guides is critical for correctly predicting plate motions (e.g., *Zhong et al.* (1998)). In order to maximize the slab sharpness, the upper mantle structure was created with slab contours from seismicity (*Gudmundsson and Sambridge*, 1998).

2.4 Results

Computed models predict velocity, viscosity, strain rate, stress magnitude, orientation of the stress axes, and energy dissipation. The models are tested by assessing the plateness of the surface velocity field, and its misfit with inferred surface velocities. The current best model has a yield stress of 100 MPa and stress exponent of 3.0 (*Stadler et al.*, 2010), with deformation highly localized around plate boundaries. Plate interiors and slabs have a viscosity of $\sim 10^{24}$ Pa s. The hinge of subducting plates yields, causing the viscosity in the hinge to drop to ~ 5

$\times 10^{22}$ to 10^{23} Pa s, consistent with estimates of *Billen et al*. (2003) and *Wu et al*. (2008). This global model allows us to study the local state of stress in a globally consistent framework, including Bolivia and Tonga.

First, we consider the region containing the 1994 M_W 8.3 Bolivia event (647 km depth), where Nazca subducts under the South-American plate at $\sim$ 8 cm/year (*Bird*, 2003). High strain rates are found exclusively in the trench, indicating highly localized deformation at the plate boundaries (Figure 2.1a). The Bolivia 1994 earthquake experienced a minimum frictional stress of 55 MPa and a static stress drop of 114 MPa (*Kanamori et al.*, 1998). This provides an estimate of the minimum stress needed in the slab. There are several other deep earthquakes with large predicted stress drops in the same region, including the 1970 Colombia (M_W 8.3) earthquake with a stress drop of 68 MPa (*Fukao and Kikuchi*, 1987; *Ruff*, 1999). The modeled slab allows for these stress drops, and shows ambient stresses that are almost everywhere equal to the yield stress, 100 MPa (Figure 2.1c). Locally, the stress is even greater, namely where the temperature is higher than the yield temperature. The modeled state of stress in the nominal model is in good agreement with earthquake focal mechanisms (Figures 2.1b and d). The stress axes indicate downdip tension in the hinge and shallow to intermediate depths in the slab, and compression in the deeper parts. This transition from tension to compression around 300 km depth is consistent with the focal mechanisms of *Isacks and Molnar* (1971).

The second case study focuses on the northern Tonga region, containing the 1994 M_W 7.6 earthquake. This is a highly complex area with several microplates and rapid trench rollback (*Bird* (2003); Figure 2.2a). The strain rate again indicates that the deformation almost exclusively occurs at plate boundaries. An additional constraint here is the estimate of a minimum average slab strain rate of 5×10^{-16} s^{-1}, determined from seismic moment release

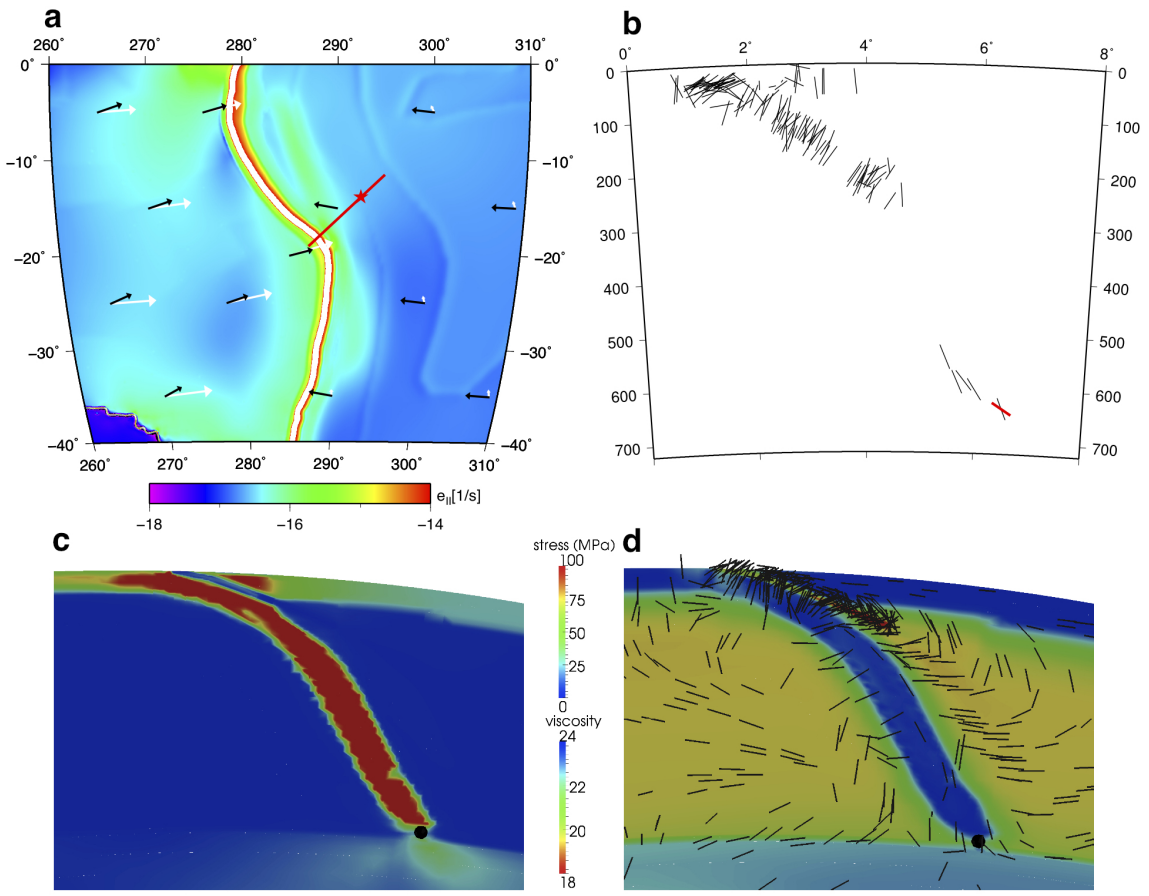

Figure 2.1. Bolivia region. (a) Map with plate motions in a no-net-rotation reference frame. Black arrows: Rhea model prediction; white arrows: Nuvel1-NNR plate motion model by *Argus and Gordon* (1991). Background color: second invariant of the strain rate. Red star: location of the Bolivia 1994 earthquake. Red line: location of the studied cross-section. (b) Cross-section with compressional axes from focal mechanisms of earthquakes with magnitude larger than 5.0 and within 100 km of the cross-section. Red axis: Bolivia 1994 event. (c) Cross-section of the stress magnitude. Black sphere: location of Bolivia 1994 event. (d) Cross-section of viscosity with compressional axes plotted with unit length.

(*Bevis*, 1988; *Holt*, 1995; *Nothard et al.*, 1996). In our nominal model, the strain rate is around or above this minimum in most of the slab, except in the plates and parts of the thicker slab interior (Figure 2.2c). The volume average of the strain rate in the slab is 7.6×10^{-16} s^{-1}, and satisfies the minimum condition. Focal mechanisms of earthquakes in this area (Figure 2.2b) show a pattern of mostly compression in the slab, except for the plate hinge and the immediate subsurface of the shallow parts of the slab. The pattern of the compressional stress axes (Figure 2.2d) matches these observations as well as inferences by *Isacks and Molnar* (1971). The gap in seismicity around 300 km depth corresponds to an area with lower strain rates, consistent with the generic models of *Vassiliou et al*. (1984).

Inspection of the stress field in models with different yield stress indicates that the orientation of the stress axes does not depend on the strength of the slab within the range of models tested. It appears that the stress orientations are determined by slab geometry rather than its strength within the range of models tested, since we see large variations in stress regime among slabs in both our models and in observations, as illustrated by the two case studies in this paper.

Global models show that a minimum value of 100 MPa for the maximum yield stress is required to acceptably fit plate motions and plateness arguments (*Stadler et al.*, 2010). A higher yield stress allows for less weakening in the hinge zone, slows the plate down, and causes lower strain rates (Figure 2.3). Studies of seismic moment release indicate that average strain rates in slabs above 175 km depth must be at least 10^{-15} s^{-1}, and below 200 km at least 5×10^{-16} s^{-1} (*Bevis*, 1988; *Holt*, 1995; *Nothard et al.*, 1996). Slab averages below 200 km depth and the value at 50 km depth for models with various yield stresses show that this provides an upper bound on the slab stress between 100 and 200 MPa (Figure 2.3a). The estimated stress drop for the Bolivia event determines a lower bound on the sustained slab

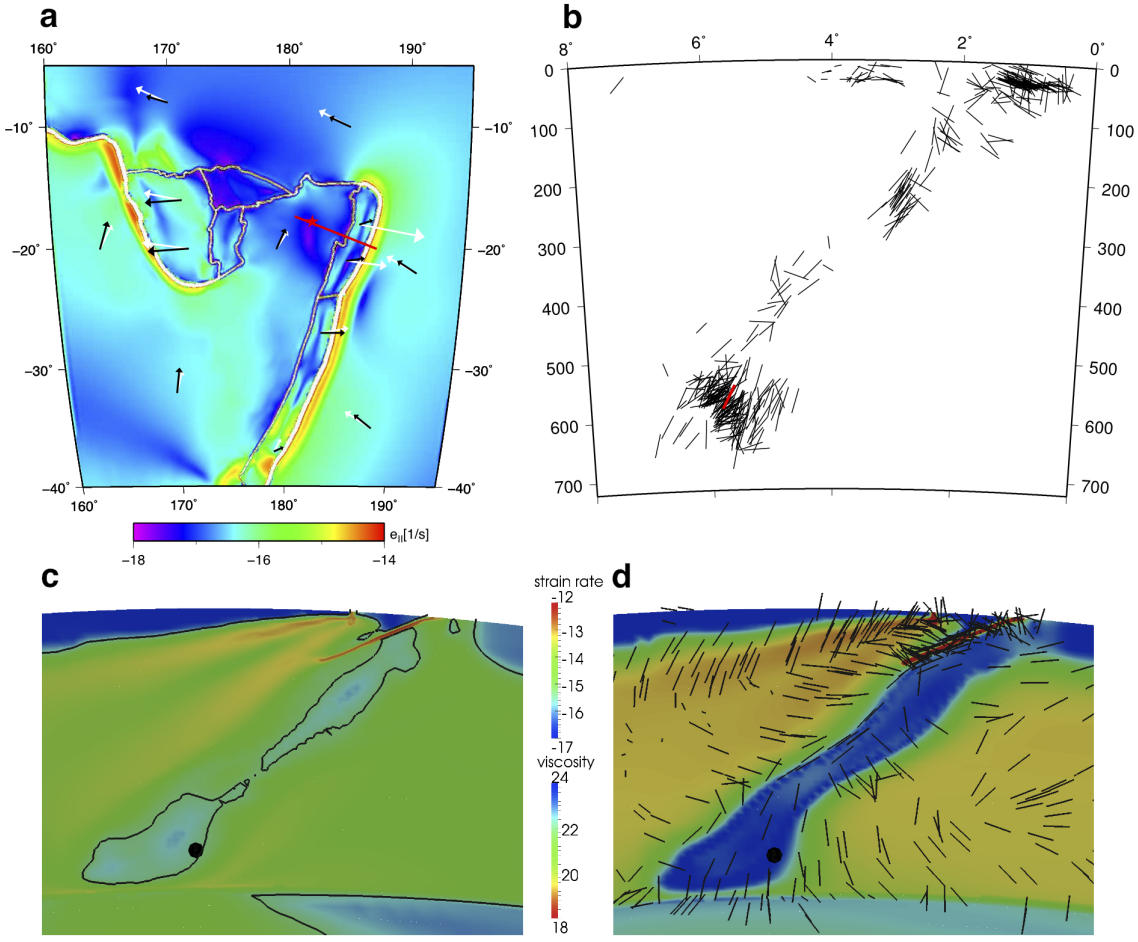

Figure 2.2. Tonga region. (a) Map with plate motions; see caption of Figure 2.1 for explanation of annotations. (b) Cross-section with compressional axes from focal mechanisms of earthquakes with magnitude larger than 5.0 and within 50 km of the cross-section. Red axis: Tonga 1994 event. (c) Cross-section of the second invariant of the strain rate. Black contour: value of 5×10^{-16} s^{-1}. (d) Cross-section of viscosity with compressional axes plotted with unit length.

stress of 100 MPa (*Kanamori et al.*, 1998) (Figure 2.3b). These requirements strongly limit the acceptable parameter space.

2.5 Discussion and Conclusions

Models with higher yield stress have higher viscosity and therefore higher ambient stress in the slab. For yield stresses larger than 200 MPa, the viscosity in the slab reaches the maximum cutoff value of 10^{24} Pa s, causing the ambient stress in the slab to be lower than the yield stress. Stress in the slab can locally be larger than the yield stress, if the temperature is higher than the yield temperature. The stress orientations do not vary between the models in this paper. However, they are dependent on radial viscosity gradients.

There are some limitations to the models presented. First, the thermal field in the upper mantle does not contain active upwellings. This could be significant in areas where plumes affect regional flow patterns. Second, the parameters used in the viscosity law are mostly established in laboratory experiments (*Hirth and Kohlstedt*, 2003), performed at low pressure and extrapolated to mantle conditions. The behavior of plates and slabs is sensitive to the choice of these parameters. Third, our models are instantaneous and hence do not include the time evolution of slabs, which would provide an additional constraint on the rheology parameters.

Stress drops of earthquakes provide a valuable constraint on the minimum stress sustained in a plate or slab. The actual stress drop on a fault can be highly heterogeneous due to spatial variability of stress and strength on the fault plane. This could result in high local stress drop compared to the average over the fault (*Venkataraman and Kanamori*, 2004). Stress drops are determined from seismic moment and rupture area, and accurately determining the rupture

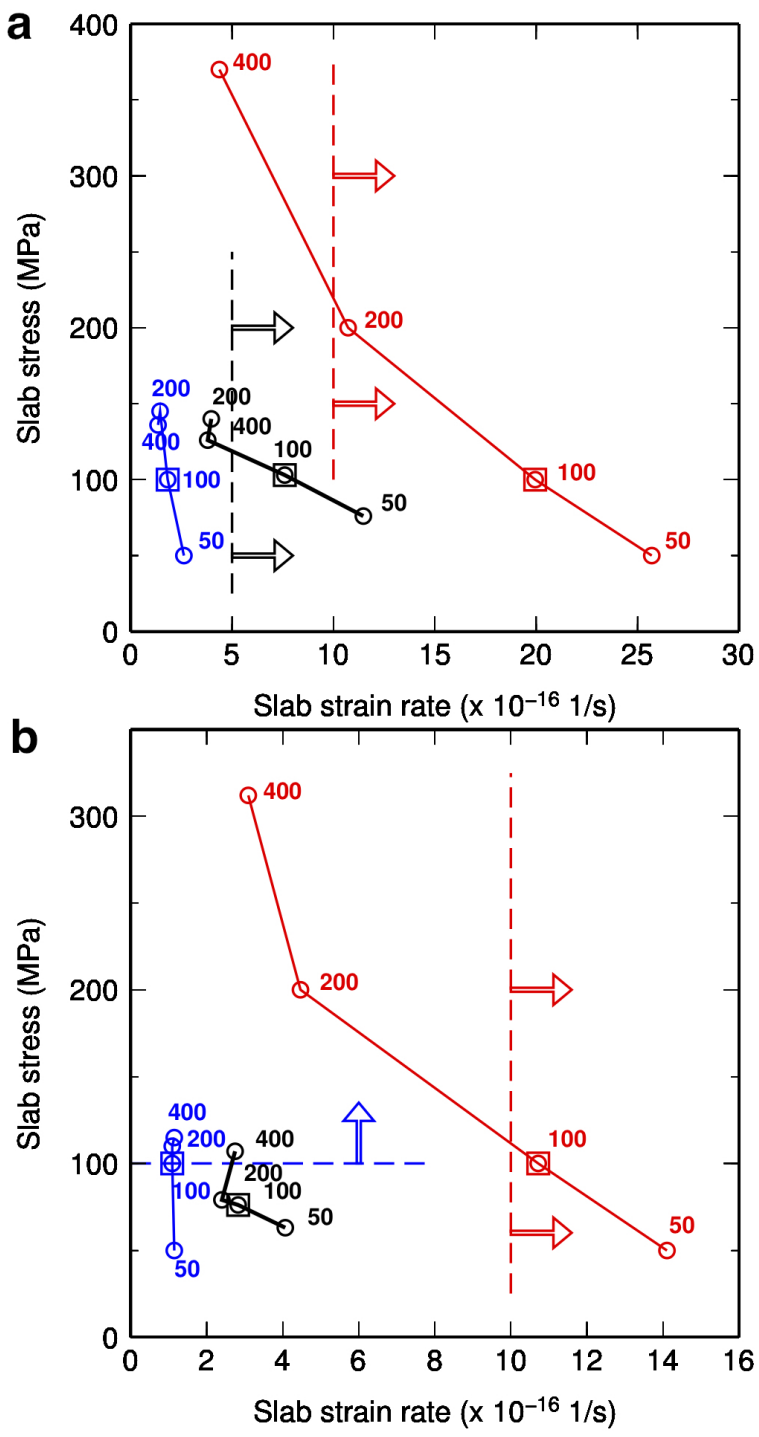

Figure 2.3. (a) Strain rate and stress in the Tonga slab. Black: average in the slab from 200 km depth to the slab tip, where the slab is defined by a viscosity contour of 5×10^{22} Pa s. Blue: value at the center of the slab at 600 km depth. Red: value at the center of the slab at 50 km depth. Square: nominal model. The numbers next to the data points refer to the global maximum yield stress used. Black dashed line: minimum average strain rate of 5×10^{-16} s^{-1} below 200 km; red line: minimum of 10^{-15} s^{-1} in the shallow slab (*Bevis*, 1988). (b) Strain rate and stress in the Bolivia slab; same color coding. Blue dashed line: minimum stress value of 100 MPa required by the stress drop at 600 km depth (*Kanamori et al.*, 1998).

area remains an active field of research (*Venkataraman and Kanamori*, 2004; *Kanamori and Brodsky*, 2004). Also, there is currently also no method available to determine how much higher the actual stress is compared to the stress drop (*Kanamori and Brodsky*, 2004). A recent study of exhumed ultramafic pseudotachylytes suggests that higher stresses could be required in slabs than previously inferred from earthquake inversions; the estimated stress drop determined from the geologic record for deep earthquakes in Corsica is at least 220 MPa, and could be as much as 580 MPa (*Andersen et al.*, 2008).

In our models, the localization of strain in the hinges of subducting slabs causes significant weakening of the material up to 2 orders of magnitude in viscosity. This process allows the rest of the slab to remain strong while still having sufficiently fast moving plates. Pointwise the dissipation of energy in the mantle is highest in the subducting plate hinges, but the integration over this very small volume compared to the rest of the mantle results in only 3%–5% of the total dissipation (*Stadler et al.*, 2010). This is consistent with findings by *Leng and Zhong* (2010).

We have studied the state of stress in slabs in globally consistent dynamic models of mantle convection with plates, and are able to reproduce the general trends in stress orientations in the Bolivia and Tonga case studies, as observed from earthquake focal mechanisms. These models have strong slabs and weak subducting plate hinges, such that the dissipation in the bending areas of plates is small compared to the total dissipation of energy from the mantle. A lower bound on the strength of slabs is provided by the stress drop in strong deep earthquakes. Because models with higher yield stress have lower strain rates in slabs, the minimum average strain rate in slabs determined from seismic moment release gives an upper bound on the strength of the slabs.

Acknowledgements

We thank H. Kanamori and D. Stegman for helpful discussions. This work was partially supported by NSF's PetaApps program (OCI-0749334, OCI-0748898), NSF Earth Sciences (EAR-0426271, EAR-0810303), and the Caltech Tectonics Observatory (by the Gordon and Betty Moore Foundation). Computing resources on TACC's Ranger and Spur systems were provided through the NSF TeraGrid under grant number TG-MCA04N026. The figures in this paper were produced using GMT and Paraview.